Journal of proteome research

pubs.acs.org/jpr

Article

# Metabolomic Nuclear Magnetic Resonance Studies at Presymptomatic and Symptomatic Stages of Huntington's Disease on a *Drosophila* Model

Marylène Bertrand,* Martine Decoville, Hervé Meudal, Serge Birman, and Céline Landon

Cite This: *J. Proteome Res.* 2020, 19, 4034–4045

Read Online

ACCESS | Metrics & More | Article Recommendations | Supporting Information

**ABSTRACT:** Huntington's disease (HD) is an inherited neurodegenerative disorder, for which diagnostic development and discovery of new therapeutic targets are urgently required. In this study, a model of HD in *Drosophila melanogaster* has been used to identify metabolic biomarkers at presymptomatic and symptomatic stages of the disease. The pan-neuronal expression of a pathogenic fragment of the human Huntingtin (HTT) protein containing a 93-repeat polyglutamine expansion (Httex1p Q93) in transgenic flies induces a neuropathology with several characteristics of the human disease. The discriminant metabolites between the diseased flies and their controls were identified by $^{1}$H nuclear magnetic resonance and orthogonal partial least squares discriminant multivariate analysis. The experiments carried out with 10-day-old flies allowed us to identify a set of 10 biomarkers of the presymptomatic stage: $NAD^{+}$, AMP, fumarate, asparagine, dimethylamine, $\beta$-alanine, glutamine, succinate, glutamate, and ethanol. Remarkably, the experiments conducted with 16-day-old flies, when the symptoms of the disease were present, highlighted a different set of 6 biomarkers: phosphocholine, ethanolamine, 2-oxoglutarate, succinate, pyruvate, and acetate. Our results provide a better understanding of the metabolic impairments in a widely used HD model and demonstrate that metabolism perturbations change dramatically during the development of the disease.

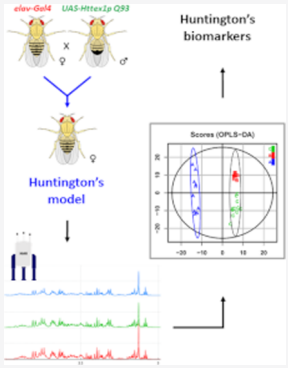


**KEYWORDS:** *Huntington's disease, neurodegenerative diseases, Drosophila, metabolomics, NMR, presymptomatic*



## INTRODUCTION

Huntington's disease (HD) is an autosomal dominant inherited neurodegenerative disorder caused by a mutation in the *huntingtin* (*HTT*) gene located at band 4p16.3 on chromosome 4.[1] Patients developing HD have an expanded CAG repeat in the first exon of the gene that includes from 36 to 121 repeats,[2] leading to polyglutamine expansion in the Huntingtin protein (HTT). Depending on the length of the CAG repeat and of other genetic and environmental conditions, symptoms usually appear between the ages of 30 to 50. These symptoms include motor dysfunction, psychiatric disturbances, and cognitive decline. The patients also develop other symptoms such as muscle atrophy, impaired glucose tolerance, and weight loss. There is currently no treatment to stop or reverse the course of the disease, which generally leads to death within 10 to 30 years after emergence.[3] However, some medications can limit the clinical defects.[4,5]

At the molecular level, the mutant Huntingtin protein (mHTT) accumulates abnormally. Misfolded fragments of this protein containing the polyglutamine expansion form cytoplasmic aggregates and nuclear inclusions throughout the brain,[6] leading to progressive neuronal toxicity. The disruption of several cellular mechanisms has been reported, including alterations in gene expression and transcription, protein folding and degradation, synaptic signaling, and energy metabolism.[7−9] To better understand the causes and consequences of the disease, different studies have been carried out on humans and animal models to discover metabolic biomarkers of HD,[10] most of them focusing on the brain, either *post mortem*[11,12] or *in vivo*.[13,14] Some metabolomic analyses have also been conducted in biological fluids such as plasma[15,16] or cerebrospinal fluid.[17] HD animal models have been developed in various organisms such as mouse,[18−20] rat,[17,21,22] sheep[23] or invertebrates such as the fruit fly *Drosophila*.[24−26]

Here, we selected *Drosophila* as this model organism is well-established to study human diseases. *Drosophila* are easy to handle and many approved genetic tools are available for transgenesis and gene expression/inactivation in specific cell and tissue types. The *Drosophila* genome is 23 times smaller than the human genome, but about 75% of the genes involved in human diseases have orthologues in *Drosophila*. Although its brain appears to be simple compared to mammals, *Drosophila* display complex behaviors such as learning and memory, sleep, or courtship.[25] In addition, its nervous system is composed of

**Received:** May 20, 2020
**Published:** September 3, 2020





https://dx.doi.org/10.1021/acs.jproteome.0c00335
*J. Proteome Res.* 2020, 19, 4034–4045

various types of neurons (dopaminergic, serotonergic, glutamatergic, GABAergic...) and glia as in vertebrates. Numerous models of neurodegenerative diseases, including Parkinson's or Alzheimer's diseases, have been developed in *Drosophila*.[27] HD models have been described by over-expressing either in the eyes, neurons, or glial cells, amino terminal fragments of human HTT containing various tracts of polyQ, or full-length human mutant HTT (128Q).[25−28] These models summarize the characteristic symptoms of HD, namely protein aggregation, neurodegeneration, behavioral defects, and reduced lifespan.

In this report, we describe the changing metabolic profile of a pan-neuronal *Drosophila* model of HD. The purpose of our study was to identify biomarkers of HD using $^{1}$H nuclear magnetic resonance (NMR) at two stages of the disease, presymptomatic and symptomatic, using 10-day-old and 16-day-old HD flies, respectively. We show that the metabolic signature of the disease is significantly different at these two stages.

## EXPERIMENTAL PROCEDURES

### *Drosophila* Culture

The fly stocks were maintained at 22 °C on a standard medium (per liter: 90.25 g of cornmeal, 82.5 g of dry yeast, 10.75 g of agar and 37.5 mL of a 10% solution of methyl-4-hydroxybenzoate in ethanol). Crosses were performed at 25 °C on a standard medium. The F1 progeny was collected each day and maintained at 25 °C on Nutri-Fly medium (Dominique Dutscher, Brumath, France). *Drosophila* lines were: $w^{1118}$ used as wild-type controls, *elav-Gal4* ($elav^{C155}$)[29] and *UAS-Httex1p Q93*.[30] To express Httex1p Q93 in neurons, *elav-Gal4* virgin females were crossed with *UAS-Httex1p-Q93* males (*HD flies*) (Figure 1). As controls, we crossed *elav-Gal4* virgins with $w^{1118}$ males (*Gal4* controls) and $w^{1118}$ virgins with *UAS-Httex1p Q93* males (*UAS* controls). Only F1 progeny females were used for metabolite analysis in this study. The analysis was carried out in females specifically because they are larger than males and heterozygous for the X-linked *elav-Gal4* insertion.

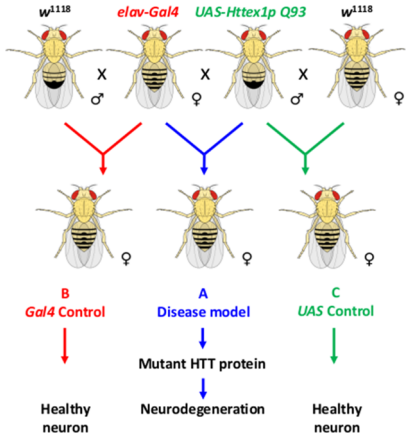


**Figure 1.** Fly crossing scheme used to generate the three sets of samples. Disease model [(A) HD flies in blue], *Gal4* control [(B) in red], and *UAS* control [(C) in green]. Only F1 progeny females of these crosses were used for this study.

### Sample Preparation

Eight to twelve samples were prepared for each batch of HD flies or controls. In order to have a good signal/noise ratio (SNR) in NMR spectra, five female *Drosophila* were used per sample. They were flash frozen in a 1 mL microtube by immersion in liquid nitrogen. Flies were then manually crushed with a suitable conical stick in the microtube and 400 μL of ice-cold 50% acetonitrile was added as described in previous studies.[31,32] The mixture was shaken with a vortex, sonicated during 5 min in an ice-cold bath and then centrifuged for 10 min at 15,300*g* at 5 °C. The supernatants (350 μL) were transferred to new tubes. Acetonitrile was evaporated in a SpeedVac for 30 min. The tube contents were freeze-dried overnight and stored at −80 °C.

For NMR analyses, 300 μL of an ice-cold 50 mM phosphate buffer (pH 7.4) in $D_2O$ containing 7.5 μg/L 3-(trimethylsilyl)-propionic-2,2,3,3-d4 acid sodium salt (TSP-D4) was added to the lyophilized samples. After homogenization with vortex, centrifugation for 10 min at 15,300*g* at 5 °C, 250 μL of the supernatant were transferred to a 3 mm NMR tube, and kept at 5 °C.

### NMR Acquisition and Processing

The NMR measurements were performed at 25 °C on a Bruker AVANCE-III HD 700 spectrometer, equipped with a 5-mm HCN triple resonance cryoprobe. Bruker's TopSpin software 3.2 package was used for the acquisition and processing of NMR spectra. $^{1}$H NMR spectra were acquired using a cpmgpr1d pulse program, which attenuates broad signals from high-molecular-weight components (D1 = 4 s; 128 scans; spectral width: 11 ppm; experimental time: 14 min). The water signal was suppressed by presaturation of the water peak. For assignment purposes, bidimensional COSY, TOCSY, and $^{13}$C-HSQC spectra were acquired (see Figure S1 in the Supporting Information). The first spectrum was manually phased. The following spectra were automatically phased and referenced to TSP resonance at 0.0 ppm and their baselines were adjusted. A moderate local baseline correction[33] and a peak alignment of the NMR spectra[34,35] was performed with NMRProcFlow open source software (https://www.nmrprocflow.org/[36]). The NMR spectra (2 zones excluding the water peak's region from 4.86 to 4.75 ppm) were segmented into variable buckets using the "intelligent bucketing" method[37] of NMRProcFlow software. The spectral regions from 1.38 to 1.25 and 0.93 to 0.85 ppm (signals of residual lipids) and the spectral regions having a SNR lower than 3 were excluded. All NMR spectra were processed with NMRProcFlow in exactly the same way so that they could be compared reliably, and were exported into a unique data matrix.

### Statistical Analysis

This data matrix was further split into three sets of data, allowing three analyses: (i) the presymptomatic analysis compares the 10-day-old fly samples, carrying the disease (HD flies) or not (controls); (ii) the symptomatic analysis compares the 16-day-old fly samples, carrying the disease or not and; (iii) the change analysis compares the HD flies at the two stages of the disease.

Each set of data was imported in Workflow4Metabolomics 3.0 Galaxy online infrastructure for the statistical analysis achievement (https://galaxy.workflow4metabolomics.org/[38]). Before the statistical analyses, the buckets in each NMR spectrum were normalized to the total sum of the spectral


https://dx.doi.org/10.1021/acs.jproteome.0c00335
J. Proteome Res. 2020, 19, 4034−4045

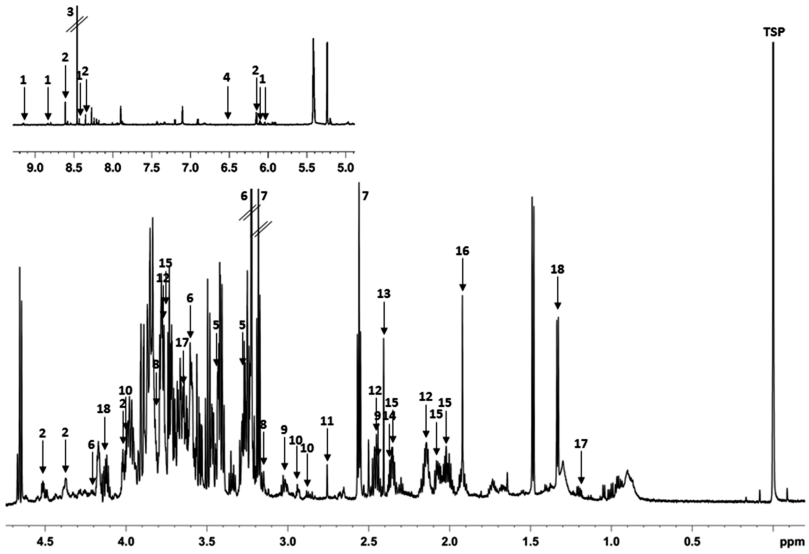


**Figure 2.** Example of $^{1}$H NMR spectrum with the identified metabolites. This spectrum was obtained with 16-day-old HD flies and is representative of spectra obtained at all stages and in control flies. (1) $NAD^{+}$ nicotinamide adenine dinucleotide—(2) AMP adenosine monophosphate—(3) formate—(4) fumarate—(5) taurine—(6) phosphocholine—(7) $\beta$-alanine—(8) ethanolamine—(9) 2-oxoglutarate ($\alpha$-ketoglutarate)—(10): asparagine—(11) dimethylamine—(12) glutamine—(13) succinate—(14) pyruvate—(15) glutamate—(16) acetate—(17) ethanol—(18) lactate.

intensity. For each set of data, multivariate, as well as univariate statistical analyses were performed to check the quality and the dispersion of samples, the quality of variables, and to find the discriminant variables between the groups.

### Multivariate Statistical Analyses

OPLS-DA (orthogonal partial least-squares discriminant analysis) was used as multivariate analysis in order to find discriminant variables of two groups of samples.[39] Three parameters were followed to evaluate the quality of OPLS-DA models: R2X and R2Y to quantify the goodness-of-fit and Q2Y to quantify predictive accuracy of the model. Permutation tests (100 cycles) were conducted to assess the robustness. Discriminant variables were defined by a threshold of variable importance of projection (VIP) coefficients in the prediction greater than one, derived from the OPLS-DA model. This method offers the advantage to remove disturbing variation.

### Univariate Statistical Analyses

Through the Workflow4Metabolomics online infrastructure[38] univariate statistical analyses were performed, in order to check the significance of the variables. The factor of interest being qualitative with two levels, *t*-test with *p*-value significance threshold of 0.05 was performed and *p*- and *q*-values were calculated.[40] The *q*-value gives the expected positive false discovery rate obtained by rejecting the null hypothesis for any result with an equal or smaller *q*-value. For metabolites with several peaks, common or average *p*- and *q*-values of the different peaks are given.

### Metabolite Identification

The NMR peaks highlighted by VIPs upper than one were then assigned. The corresponding metabolites were identified from their $^{1}$H and $^{13}$C chemical shifts, with databases such as HMDB,[41] BRMB,[42] and a home-made database. For unambiguous identifications, when needed, some reference compounds were directly added to the samples to identify precisely the affected peaks of interest. It is worth mentioning that metabolites displaying several peaks in the $^{1}$H NMR spectrum were retained only when all of the peaks were present and when all or most of the peaks were discriminant.

### Discrimination Performance of Biomarkers

Using open source MetaboanalystR software[43] (https://www.metaboanalyst.ca) prediction models and ROC (receiver operating characteristic) curves were performed to identify a set of metabolites capable of classifying unknown samples as HD or control samples with high sensitivity and specificity. A matrix composed of all samples (10- and 16-day-old HD and control flies) and of the 46 variables/peaks of the discriminating metabolites was created and ROC curves were constructed to select the best metabolite combination. A model with 15 metabolites (one variable by metabolite) was created. Finally, the performance of the model was evaluated with ROC curve and logistic regression analyses were performed with selected variables and samples.

## RESULTS

Nervous system expression of the first exon of human HTT with 93 CAG repeats (*Httex1p Q93*) has been extensively characterized in previous works as a reliable HD model in *Drosophila*.[30,44−49] Here, we used *elav-Gal4* as a driver, allowing expression of the polyglutaminated protein in all neurons which causes reduced viability and neuronal degeneration in adult flies. Because *Httex1p Q93* was not only expressed in the brain but also in the ventral nerve cord and peripheral neurons with this driver, metabolites were extracted from the entire *Drosophila* and not only from the head. In this study, we performed NMR experiments on 10- and 16-day-old HD flies and on their two controls: 10-day-old flies are at a presymptomatic stage, as indicated by the fact that they do not show a significantly higher death rate than the controls, while the survival of 16-day-old HD flies is reduced to about 50% of that of the controls, indicating that they have reached a fully symptomatic stage.[45] A typical NMR spectrum obtained with 16-day-old HD flies is shown in Figure 2.


https://dx.doi.org/10.1021/acs.jproteome.0c00335
J. Proteome Res. 2020, 19, 4034−4045

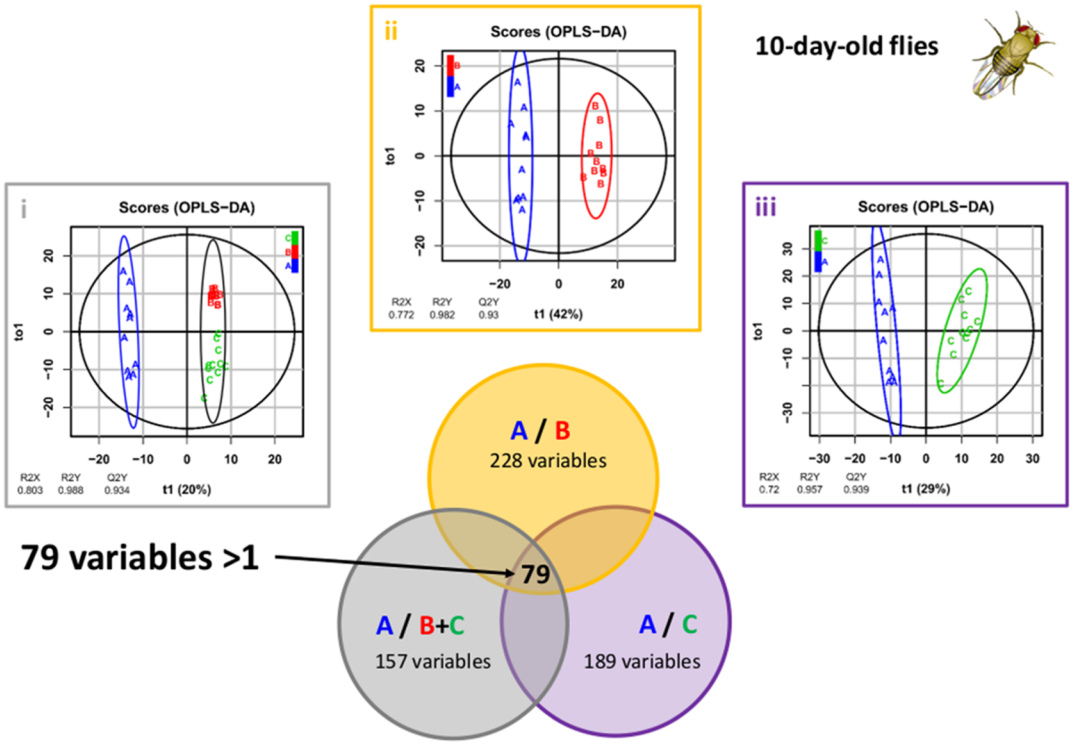


**Figure 3.** Discriminant variables at the presymptomatic stage (10-day-old flies). OPLS-DA analyses performed between the three groups of samples of 10-day-old flies. (i): OPLS-DA analysis for discrimination of HD flies and sum of *Gal4* and *UAS* controls; (ii): OPLS-DA analysis for discrimination of HD flies and *Gal4* controls; (iii): OPLS-DA analysis for discrimination of HD flies and *UAS* controls. A Venn diagram shows the 79 variables common to the three sets of samples. A: HD flies (in blue), B: *Gal4* controls (in red), and C: *UAS* controls (in green).

To eliminate the contribution of each transgene to modifications of the metabolite patterns, two controls were processed in parallel. The first one corresponds to flies carrying only the *elav-Gal4* transgene (*Gal4* control) and the second one to flies carrying only the *UAS-Httex1p Q93* transgene (*UAS* control). For each experiment, statistical analysis was performed by comparing HD flies with *Gal4* controls then with *UAS* controls, and finally HD flies with the associated *Gal4* and *UAS* controls. Only VIPs common to the three comparisons were retained for further analysis. This method excludes the variables which are discriminant for one type of controls only and keeps the most reliable variables.

## Presymptomatic Stage Biomarkers

An OPLS-DA model was used to find the discriminant metabolites between the 10-day-old HD flies and the controls (Figure 3). Only discriminant variables (VIPs > 1) from OPLS-DA and showing confidence interval at the 95% level were retained: (i) 157 variables were identified between HD flies and the associated two controls, (ii) 228 variables between HD flies and *Gal4* controls, and finally (iii) 189 variables between HD flies and *UAS* controls. All of the OPLS-DA analyses performed led to a good or excellent separation of the groups and had large R2X (0.80; 0.77 and 0.72, respectively) and R2Y (0.99; 0.98 and 0.96, respectively), which indicated high reproducibility and a good fitting of the model to the data. The Q2Y parameters, calculated by cross validation were close to 1 (0.93; 0.93 and 0.94, respectively) which are indicative of the high predictivity of the models. The discriminant variables of the three OPLS-DA were compared to each other using a Venn diagram and the 79 variables common to the three groups were retained for further analysis.

The metabolites identified for the 10-days-old flies from the 79 discriminant variables are presented in Table 1 (VIP score of each of the discriminant metabolites is shown in the Figure S2 as the Supporting Information). All of the *q*-values are very low, which means that the identified metabolites are statistically highly significant. At this stage of the disease, all the identified metabolic biomarkers are lower in HD flies than in controls.

## Symptomatic Stage Biomarkers

The same procedure as for the 10-day-old flies was conducted for the 16-day-old flies (Figure 4). The discriminant variables (VIPs) > 1 from OPLS-DA and showing confidence interval at the 95% level were retained: (i) 156 variables were found between HD flies and the associated two controls, (ii) 136 variables between HD flies and *Gal4* controls and finally (iii) 191 variables between HD flies and *UAS* controls. All of the OPLS-DA analyses performed lead to a good or excellent separation of the groups. Correct R2X (0.57; 0.71 and 0.50, respectively) and large R2Y (0.95; 0.99 and 0.98, respectively) indicated high reproducibility and a good fitting of the model to the data. Q2Y parameters were calculated by cross validation and were close to 1 (0.87; 0.89 and 0.97, respectively), which demonstrates the high predictivity of models. Furthermore, the discriminant variables produced by the three OPLS-DA analyses were compared to each other using a Venn diagram and the 46 common variables were retained.

Only six metabolites were unambiguously identified from the 46 discriminant variables, and are presented in Table 2 (the VIP score of each of the discriminant metabolites is shown in the Figure S3 as the Supporting Information). Note that at this


https://dx.doi.org/10.1021/acs.jproteome.0c00335
J. Proteome Res. 2020, 19, 4034−4045

**Table 1. Metabolites Identified from the 79 Common Discriminant Variables with VIP > 1, for the 10-Day-Old Flies[a]**

| 10-day-old | $^1$H chemical shift in ppm (multiplicity) | assignment | *q*-value | *p*-value | | |
|---|---|---|---|---|---|---|
| $NAD^+$ | | | **** | | ↓ | |
| | 9,35 (s) | nicotinamide CH | | | | |
| | 9,15 (d) | nicotinamide CH | **** | **** | ↓ | |
| | 8,84 (d) | nicotinamide CH | **** | **** | ↓ | |
| | 8,43 (s) | adenine CH | | | | ov |
| | 8,20 (dd), 8,18 (s) | adenine CH | **** | **** | ↓ | |
| | 6,10 (d) | ribose CH | **** | **** | ↓ | |
| | 6,05 (d) | ribose CH | **** | **** | ↓ | |
| | 4,55 (m) | ribose CH | **** | **** | ↓ | ov |
| | 4,52 (dd) | ribose CH | **** | **** | ↓ | ov |
| | 4,50 (m) | ribose CH | **** | **** | ↓ | ov |
| | 4,43 (m) | ribose CH | **** | **** | ↓ | ov |
| | 4,38 (m) | ribose CH | **** | **** | ↓ | ov |
| | 4,37 (m) | ribose CH | | | | ov |
| | 4,27 (m) | $CH_2$ | **** | **** | ↓ | ov |
| | 4,25 (m), 4,22 (m) | $CH_2$ | **** | **** | ↓ | ov |
| AMP | | | **** | **** | ↓ | |
| | 8,61 (s) | adenine CH | **** | **** | ↓ | |
| | 8,26 (s) | adenine CH | | | | ov |
| | 6,15 (d) | ribose CH | **** | **** | ↓ | |
| | 4,52 (dd) | ribose CH | **** | **** | ↓ | ov |
| | 4,38 (m) | ribose CH | **** | **** | ↓ | ov |
| | 4,02 (m) | $CH_2$ | **** | **** | ↓ | ov |
| fumarate | | | **** | **** | ↓ | |
| | 6,52 (s) | CH | **** | **** | | |
| asparagine | | | **** | **** | ↓ | |
| | 4,01 (dd) | CH | **** | **** | ↓ | ov |
| | 2,95 (dd); 2,86 (dd) | $CH_2$ | **** | **** | ↓ | |
| dimethylamine | | | **** | **** | ↓ | |
| | 2,71 (s) | $CH_3$ | **** | **** | ↓ | |
| $\beta$-alanine | | | **** | **** | ↓ | |
| | 3,18 (t) | $\beta$-$CH_2$ | **** | **** | ↓ | |
| | 2,56 (t) | $\alpha$-$CH_2$ | **** | **** | ↓ | |
| glutamine | | | **** | **** | ↓ | |
| | 3,77 (t) | $\alpha$-CH | | | ↓ | ov |
| | 2,45 (m) | $\gamma$-$CH_2$ | **** | **** | ↓ | ov |
| | 2,14 (m) | $\beta$-$CH_2$ | **** | **** | ↓ | ov |
| succinate | | | ** | *** | ↓ | |
| | 2,41 (s) | $CH_2$ | ** | *** | ↓ | |
| glutamate | | | *** | **** | ↓ | |
| | 3,76 (dd) | $\alpha$-CH | | | | ov |
| | 2,35 (m) | $\gamma$-$CH_2$ | *** | **** | ↓ | ov |
| | 2,11 (m) | $\beta$-$CH_2$ | **** | **** | ↓ | |
| ethanol | | | **** | **** | ↓ | |
| | 3,66 (q) | $CH_2$ | | | | ov |
| | 1,18 (t) | $CH_3$ | **** | **** | ↓ | |

[a]Downward arrows (↓) indicate that the ratio of metabolite was lower for HD flies than for controls. s—singlet, d—doublet, dd—doublet of doublet, t—triplet, m—multiplet. **0.001 < value < 0.01; ***0.0001 < value < 0.001, ****value < 0.0001.

stage of the disease, four metabolic biomarkers have increased in HD flies, whereas two have decreased.

## Analysis of Biomarker Change

In order to follow the change of the identified metabolites with the progression of the disease, the comparison of 10-day-old and 16-day-old HD flies was carried out. The OPLS-DA analysis highlighted 177 discriminant variables (Figure 5), making it possible to identify 15 metabolites (Table 3). Note that all the metabolites previously identified (Tables 1 and 2) were discriminant between 10- and 16-day-old flies, with the exception of pyruvate. Taurine, which was not identified in the previous analysis, is now discriminant between 10- and 16-day-old HD flies.

To make sure that the change of biomarkers is well-correlated with the progression of the disease and not with the age of flies, the same analysis was performed between 10- and 16-day-old control flies. Results are presented in Table 3. We observed that three metabolites (glutamate, acetate, and ethanol) changed in the same way in diseased and control flies according to age.



https://dx.doi.org/10.1021/acs.jproteome.0c00335
J. Proteome Res. 2020, 19, 4034−4045

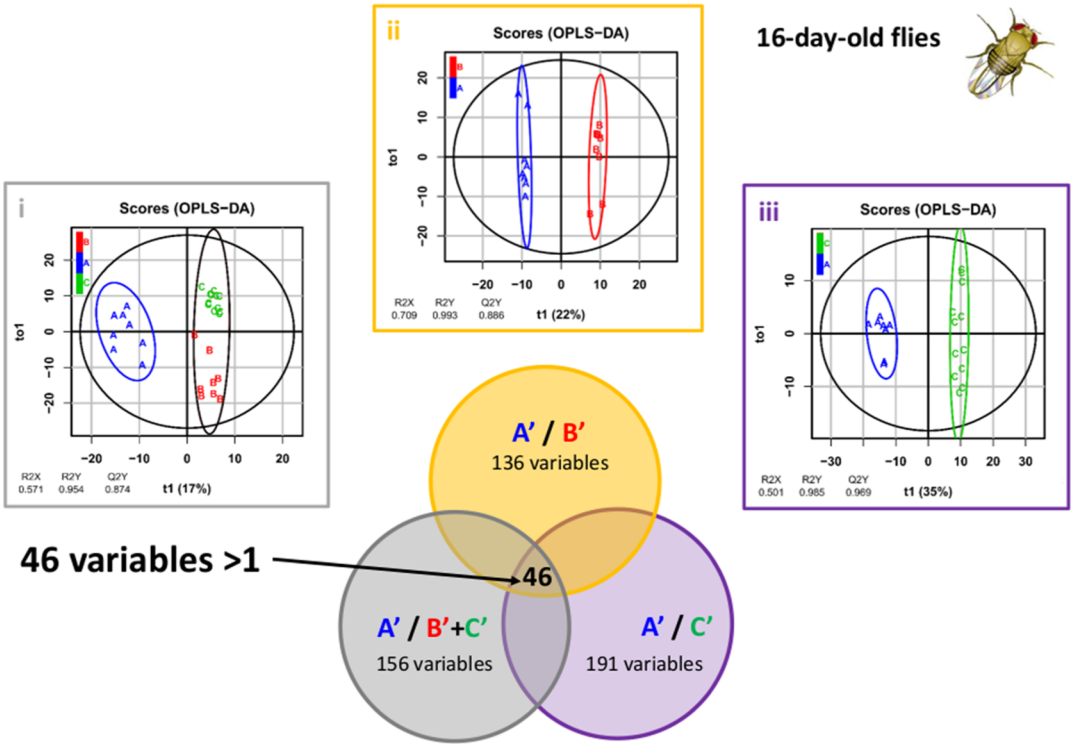


**Figure 4.** Discriminant variables at the symptomatic stage (16-day-old flies). OPLS-DA analyses performed between the three groups of samples of 16-day-old flies. (i): OPLS-DA analysis for discrimination of HD flies and sum of *Gal4* and *UAS* controls; (ii): OPLS-DA analysis for discrimination of HD flies and *Gal4* controls; (iii): OPLS-DA analysis for discrimination of HD flies and *UAS* controls. A Venn diagram shows the 46 variables common to the three sets of samples. A′: HD flies (in blue), B′: *Gal4* controls (in red), and C′: *UAS* controls (in green).

**Table 2. Metabolites Identified from the 46 Common Discriminant Variables with VIP > 1, for the 16-Day-Old Flies**[a]

| 16-day-old | $^1$H chemical shift in ppm (multiplicity) | assignment | *q*-value | *p*-value | | |
|---|---|---|---|---|---|---|
| phosphocholine | | | *** | **** | ↑ | |
| | 4,17 (m) | $CH_2$ | **** | **** | ↑ | |
| | 3,60 (m) | $CH_2$ | **** | **** | ↑ | ov |
| | 3,23 (s) | $CH_3$ | *** | **** | ↑ | |
| ethanolamine | | | **** | **** | | |
| | 3,81 (t) | $CH_2$ | **** | **** | ↑ | |
| | 3,12 (t) | $CH_2$ | **** | **** | ↑ | ov |
| 2-oxoglutarate ($\alpha$-KG) | | | ** | ** | ↓ | |
| | 3,00 (t) | $\beta$-$CH_2$ | ** | ** | ↓ | |
| | 2,44 (t) | $\alpha$-$CH_2$ | ** | ** | ↓ | ov |
| succinate | | | * | * | ↑ | |
| | 2,41 (s) | $CH_2$ | * | * | ↑ | |
| pyruvate | | | ** | *** | ↓ | |
| | 2,38 (s) | $CH_3$ | ** | *** | ↓ | |
| acetate | | | ** | ** | ↑ | |
| | 1,92 (s) | $CH_3$ | ** | ** | ↑ | |

[a]For metabolites with several peaks, the *q*-value is common to the different peaks. Downward arrows (↓) and upward arrows (↑) indicate that the proportion of metabolites was lower or, respectively, higher for HD flies than for controls. s—singlet, t—triplet, m—multiplet, ov—overlapped. *0.01 < value < 0.05; **0.001 < value < 0.01; ***0.0001 < value < 0.001, value < 0.0001.

## Discrimination Performance of Biomarkers

We have performed ROC analysis to evaluate the predictive value of the discriminant metabolites. ROC curves were constructed with different combination (2 to 46 variables). The results of multi-ROC analyses showed that the models with 10 or more variables have an area under the curve (AUC) greater than 95% (see Figure S4 as the Supporting Information). The AUC value close to one shows high sensitivity and specificity of the model. Then, a set of 15 discriminant metabolites were manually selected based on their LASSO frequencies and of their mean importance measures (phosphocholine, glutamine, pyruvate, taurine, $\beta$-alanine, succinate, acetate, 2-oxoglutarate, ethanol, ethanolamine, $NAD^+$, AMP, fumarate, glutamate, and dimethylamide). The significance of this biomarker model was evaluated using the ROC curve and logistic regression (Figure S5 as the Supporting Information). Then, different sets of samples were tested to see if the set of the 15 variables was able to sort


https://dx.doi.org/10.1021/acs.jproteome.0c00335
J. Proteome Res. 2020, 19, 4034−4045

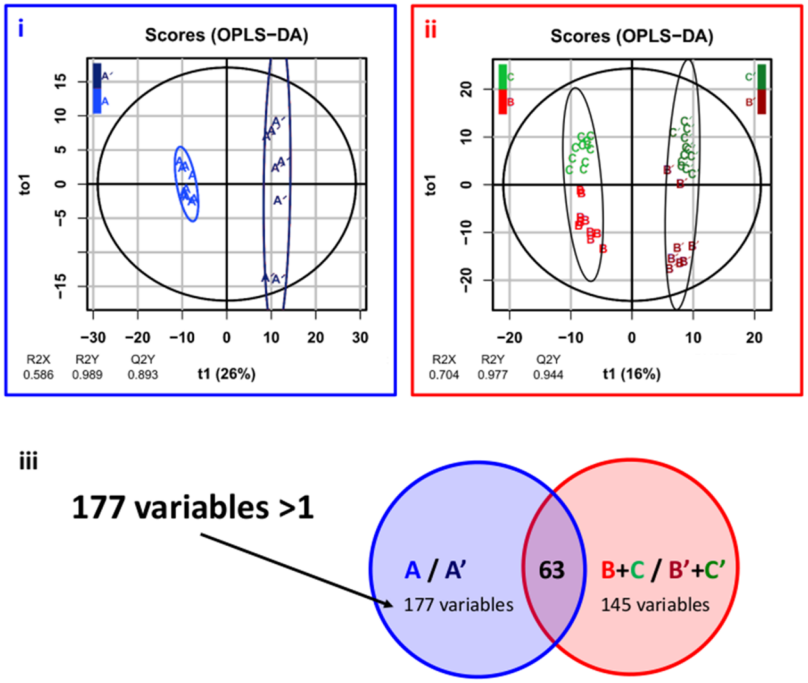


**Figure 5.** Discriminant variables over the course of the disease (10- and 16 day-old flies). OPLS-DA analyses performed between the samples of 10- and 16-day-old flies. (i): OPLS-DA analysis for discrimination of 10-day-old HD flies and 16-day-old HD flies; (ii): OPLS-DA analysis for discrimination of 10-day-old *UAS* and *Gal4* controls and 16-day-old *UAS* and *Gal4* controls; (iii): Venn diagram shows the 177 variables characteristic of the evolution of the disease. The 63 common variables are characteristic of the progression of the disease and of the age. A and A′: HD flies at 10- and 16-day old, respectively (in light and dark blue), B and B′: *Gal4* controls at 10- and 16-day old, respectively (in light and dark red) and C and C′: *UAS* controls at 10- and 16-day old, respectively (in light and dark green).

**Table 3. Metabolites Changing with HD Disease Stage and/or with Age**[a]

| 10/16-day-old HD flies | *q*-value | *p*-value | evolving with HD | *q*-value | *p*-value | evolving with age |
|---|---|---|---|---|---|---|
| $NAD^+$ | * | * | ↑ | | | |
| AMP | * | * | ↑ | *** | *** | ↓ |
| fumarate | * | * | ↑ | | | |
| taurine | **** | **** | ↑ | | | |
| phosphocholine | ** | *** | ↑ | | | |
| ethanolamine | ** | ** | ↑ | | | |
| 2-oxoglutarate | ** | *** | ↓ | | | |
| asparagine | * | ** | ↑ | **** | **** | ↓ |
| dimethylamine | ** | *** | ↑ | | | |
| *β*-alanine | ** | ** | ↑ | | | |
| glutamine | * | * | ↑ | *** | *** | ↓ |
| succinate | ** | ** | ↑ | | | |
| glutamate | * | * | ↓ | **** | **** | ↓ |
| acetate | *** | **** | ↑ | ** | ** | ↑ |
| ethanol | **** | **** | ↓ | **** | **** | ↓ |

[a]Downward arrows (↓) and upward arrows (↑) indicate that the proportion of metabolites was lower or, respectively, higher for 10-day-old than for 16-day-old HD flies. *0.01 < value < 0.05; **0.001 < value < 0.01; ***0.0001 < value < 0.001; ****Value < 0.0001.

the HD samples from the controls. The predicted class probabilities for each sample showed a good classification accuracy where 29 out of 30 samples were correctly classified (example on Figure S6 as the Supporting Information).

## DISCUSSION

In this study, a transgenic model of HD in *Drosophila melanogaster* has been used to identify metabolic biomarkers at presymptomatic (10-day-old flies) and symptomatic (16-day-old flies) stages of the disease. Our study has been performed on the whole body of the flies because in this model the mutant HTT has been expressed in all fly neurons, which are present in the head as components of the brain, but also in other parts of the fly body, such as the ventral nerve cord in the thorax or the enteric nervous system in the abdomen. A complete analysis of HD-associate defects in our model therefore required to study metabolites in the entire fly. Moreover, brain activity and state are known to influence the physiology of the whole organism, both under health and disease conditions. The discriminant metabolites between the disease carrier flies and their controls were identified by $^1$H NMR and OPLS-DA multivariate analyses. This allowed a better understanding of the metabolic impairments associated


https://dx.doi.org/10.1021/acs.jproteome.0c00335
J. Proteome Res. 2020, 19, 4034−4045

with the disease and to follow the metabolite disturbance over its progression.

The three statistical analyses reported here enabled us to: (i) identify 10 biomarkers of the presymptomatic stage; (ii) identify 6 biomarkers of the symptomatic stage and finally, (iii) monitor the change of these biomarkers during HD-like pathogenesis. It is worth mentioning that some metabolites could not be unambiguously identified from discriminant variables. Therefore, the final lists of metabolites only report the compounds that we could identified with certainty. Moreover, the regions corresponding to residual lipid peaks in NMR spectra were removed from the matrix before the statistical analyses, in order not to affect the results. As a consequence, the lactate peaks, at 1.33 and 1.35 ppm, could not be considered in our work, although lactate is a known HD biomarker, which has been highlighted in several previous studies.[17,24,50]

The discriminating performance of these metabolites was tested on the whole samples by an exploratory analysis using multivariate ROC curves. A minimum of ten metabolites is required to have a good discriminant ability. A set of 15 metabolites allows to class between HD and control samples with a good accuracy and to predict them.

The metabolites identified in our study can be classified in three groups: (i) the first group includes the metabolites directly involved in energy metabolism [fumarate, succinate, 2-oxoglutarate (or $\alpha$-ketoglutarate), pyruvate, acetate, $NAD^+$, and AMP], (ii) the second group corresponds to amino acids and derivatives (glutamate, glutamine, asparagine, $\beta$-alanine, and taurine), and (iii) the third group corresponds to miscellaneous metabolites (dimethylamine, acetate, phosphocholine, ethanol, and ethanolamine). Most of these discriminant metabolites have been reported in the literature as biomarkers of HD, in particular glutamate,[13,14,51,52] glutamine,[12,13,17,20,24,50,52,53] phosphocholine,[13,15,16,23] acetate,[50,53] succinate,[17,24,53] and pyruvate.[24,54,55] Other metabolites, such as leucine, isoleucine, valine,[23,56,57] myo-inositol,[11,58,59] *N*-acetyl-aspartate,[14,58,60] $\gamma$-aminobutyric acid (GABA)[10,12,22] were quite often pointed out, but they did not appear as discriminant in our analyses. The closest report to our study is the recent work of Singh and collaborators[24] on a *Drosophila* model of HD displaying retinal deformations. Among the metabolites, they identified by NMR analysis performed on methanolic extracts of heads, four are common to ours: $NAD^+$, pyruvate, succinate, and glutamine. These authors used the *GMR-Gal4* driver, which selectively expresses in the fly compound eyes, explaining why the analysis was focused on heads, unlike our model, in which mutant HTT is expressed in all neurons present over the entire body. Our analysis was carried out, therefore, on a larger diversity of neuronal subtypes than that used in Singh's study. The eye photoreceptors are highly specialized cells that are different from all other neurons, so one can expect that the results obtained in the retina will not be identical to those obtained in brain or other tissues. However, it is interesting to note the similarities between our results and those of Singh et al., particularly regarding energetic pathways.

Brain energy supply is well-known to be dysfunctional in HD.[61,62] Numerous evidence suggests a dysfunction of mitochondria in HD, and more specifically of the electron transport chain. However, other energy generating pathways are also implicated. In particular, the tricarboxylic acid (TCA) cycle is disrupted,[17,63] and compensatory pathways are used to fuel the TCA cycle, such as fatty acid oxidation or glutamate oxidation, for example. It has been shown that increasing glucose transport in neurons significantly enhanced *Drosophila* survival in the Httex1p Q93 model.[48] The same authors observed that overexpression of glucose-6-phosphate dehydrogenase (G6PD), the key enzyme in the pentose phosphate (PPP) pathway, also markedly extended the lifespan of HD flies. Our results highlight metabolites involved in such bioenergetic pathways: fumarate, succinate, and 2-oxoglutarate, which are intermediates of the TCA cycle, and pyruvate, which is the end product of glycolysis. Acetate is also involved in energy metabolism as it may derived from fatty acid oxidation, a pathway used when carbohydrates are low. Polyzos et al. showed in a mouse model of HD [HdhQ(150/150)] that the level of glucose was lower in the striatum of HD mice, and that astrocytes reprogramed their metabolism to use fatty acids as a fuel.[64] $NAD^+$ and $NADP^+$ are coenzymes in enzymatic oxidation−reduction (redox) reactions such as glycolysis and the TCA cycle. They are also involved in the electron transport chain. A decrease in $NAD^+$ was already noted in two studies with two different animal models of HD: *Drosophila*[24] and the mouse.[65]

Among the amino acids identified at presymptomatic stage, glutamate, and glutamine are nonessential amino acids, which are involved in brain functions. In neurons, glutamate acts as an excitatory neurotransmitter. In astrocytes, it is used to produce glutamine, which is transported into neurons and then converted into glutamate. However, glutamate may also participate to fuel the TCA cycle by generating 2-oxoglutarate. At 10 days, HD flies have a lower level of glutamate and glutamine than controls, which may suggest that these two amino acids are preferentially used to produce energy. We also noticed a decrease in asparagine at the presymptomatic stage. This was already reported in the metabolic profiling of presymptomatic HD in sheep[23] and in the plasma of HD patients.[66] Similar to glutamate, asparagine can also participates in the energy metabolism as an intermediate of oxaloacetate.

Finally, other metabolites such as phosphocholine and ethanolamine were found to increase at symptomatic stage in our model. They are precursors of phosphatidylcholine and phosphatidylethanolamine, which are major components of cellular and mitochondrial membranes and more specifically of the neuronal membranes. The increase in phosphocholine and ethanolamine observed in this study likely reflects therefore an altered turnover of membranes resulting from neurodegeneration. Alterations in phosphocholine levels have previously been reported in the blood of HD patients[15] and in various mouse models.[13,67,68]

HD is a progressive disease that gets worse with age and it is tempting to think that metabolic alterations will also worsen with age. However, Dubinsky[63] suggested that the compensation phenomena that arise in HD evolve in the course of the disease. In this study, we have highlighted the discriminating metabolites in presymptomatic and symptomatic flies. Comparative analysis between the 10-day-old HD flies and 16-day-old HD flies identifies 15 discriminants metabolites. With the exception of taurine, these metabolites are those identified in 10-day-old and 16-day-old HD flies. Among them, nine were not discriminant between 10-day-old and 16-day-old control flies (see Table 3). The variation in the level of the three metabolites glutamate, acetate, and ethanol tends to suggest that their evolution is more a consequence of age


https://dx.doi.org/10.1021/acs.jproteome.0c00335
J. Proteome Res. 2020, 19, 4034−4045

rather than of the course of the disease. The other metabolites were discriminant only in 10-day-old HD flies or only in 16-day-old HD flies. For example, fumarate has a lower level when compared with controls in 10-day-old HD flies, but was not discriminant when the 16-day-old HD flies were compared to their controls. These results suggest that discriminating metabolites at 10 days returned to a normal level at 16 days and that new discriminating metabolites appeared at this stage. Regarding succinate, its level changes in the opposite direction compared to the controls between these two stages, decreasing in 10-day-old HD flies, but increasing in 16-day-old HD flies. It is interesting to note that taurine is not discriminant when comparing 10-day-old and 16-day-old HD flies with their controls, but emerges as a discriminating metabolite when comparing 10-day-old and 16-day old HD flies. The discriminating metabolites retained in the results are those common from the three comparison pairs HD flies/*Gal4* controls, HD flies/*UAS* controls, and HD flies/sum of controls, as indicated. In this case taurine was not discriminant, but when comparing 10-day-old and 16-day-old HD flies only with the sum of the controls or only with the *Gal4* control taurine was discriminant, its level being lower in 10-day-old HD flies and higher in 16-day-old HD flies. If the taurine level changes in an opposite direction in 10-day-old and 16-day-old HD flies, taurine can become a discriminating metabolite between these two stages of the disease.

Taurine is a sulfur-containing amino-acid displaying multiple functions.[22,56,59] It is involved in brain development, neuromodulation, osmoregulation, stabilization of membranes, inflammation, neuroprotection and it has also an antioxidant function.[69] Recently, it has been shown that taurine has a protective effect in models of neurodegenerative disorders and in particular in a rat HD model.[70,71] The change in the taurine level during the progression of the disease in our *Drosophila* model, could reflect this role in neuroprotection.

As a whole, our results describe that some metabolites decrease at early stage and increase at a later stage, demonstrating that the impairments in metabolite pathways change over the course of the disease. Such observations have already been noted in the literature.[63,64] A majority of the metabolites identified in this study are related to the energy metabolism, they are intermediates of the TCA cycle or intermediates of compensatory energy mediating pathways such as fatty acid oxidation or oxidative glutamate pathway. During the progression of the disease, the cells adapt their metabolism to compensate the deficit in energy, but adopt different compensatory pathways based on accumulated metabolic and transcriptional alterations. The different energy supply pathways are tightly regulated and interconnected. For example, AMP activates several enzymes of the TCA cycle (pyruvate dehydrogenase, citrate synthase, and isocitrate dehydrogenase) and the ratio $NAD^+$/NADH influences the pyruvate/lactate ratio.[63] Other studies have reported different expression rates of enzymes involved in energy biosynthesis pathways. For example, Zabel et al.[72] have shown the up-regulation of enzymes involved in glycolysis and gluconeogenesis in 2 weeks R6/2 mice. Using the same model, Perluigi et al.[73] have demonstrated an increasing expression level of dihydrolipoamide *S*-succinyl-transferase and aspartate amino-transferase over the course of disease (10-week-old mice) and a decrease in pyruvate dehydrogenase expression level in 10-week-old HD transgenic mice compared with young (4-week-old) mice. In addition, expression of mHTT may affect transcriptional activity and may result in alteration in expression of proteins involved in the energy metabolism as demonstrated by Naia et al.[74] who found in striatal $HdhQ^{111/111}$ cells an increase of pyruvate dehydrogenase kinase expression leading to a decrease of pyruvate dehydrogenase activity.

## CONCLUSIONS

In HD, changes in metabolite levels precede structural brain alterations. Therefore, the study of molecular biomarkers at a presymptomatic stage is essential to understand better the pathogenesis and to find new therapeutic targets. Our work identifies 16 discriminatory metabolites at presymptomatic and symptomatic stages of HD modeled in *Drosophila melanogaster*. These metabolites confirm dysfunctions in energy production leading to mitochondrial dysfunction and a disruption of glycolysis, TCA, and glutamate−glutamine cycles. Our results suggest that a set of 15 metabolites characteristic of both stages of the disease could be used to distinguish HD flies from controls, indicating that they have a predictive value. As defined here on a *Drosophila* model, among this 15 metabolites, nine metabolites, namely, $NAD^+$, fumarate, taurine, ethanolamine, dimethylamine, $\beta$-alanine, succinate, phosphocholine, and 2-oxoglutarate, whose variations were found to be independent of age, may be considered first to follow the progression of HD in flies. They could be considered as potential candidates to be tested in other HD models and in human patients.

## ASSOCIATED CONTENT

### Supporting Information

The Supporting Information is available free of charge at https://pubs.acs.org/doi/10.1021/acs.jproteome.0c00335.

$^{13}$C-HSQC spectra of 16-day-old HD flies; VIP score of the metabolites for the 10-day-old flies extracted from the OPLS-DA table; VIP score of the metabolites for the 16-day-old flies extracted from the OPLS-DA table; plot of ROC curves for several biomarker models based on their average performance; plot of the ROC curve for the 15 biomarker model; and predicted class probability plots (average of the cross-validation) for each of the 30 samples using the base classifier (based with 15 metabolite variables) (PDF)

## AUTHOR INFORMATION


### Corresponding Author

**Marylène Bertrand** − *Center for Molecular Biophysics, CBM, UPR 4301, CNRS, F-45071 Orléans Cedex 02, France;* orcid.org/0000-0001-5647-5564; Email: marylene.bertrand@cnrs-orleans.fr

### Authors

**Martine Decoville** − *Center for Molecular Biophysics, CBM, UPR 4301, CNRS, F-45071 Orléans Cedex 02, France; University of Orléans, F-45100 Orléans, France*

**Hervé Meudal** − *Center for Molecular Biophysics, CBM, UPR 4301, CNRS, F-45071 Orléans Cedex 02, France*

**Serge Birman** − *GCRN Team, Brain Plasticity Unit, UMR 8249, CNRS, ESPCI Paris, PSL Research University, F-75005 Paris, France;* orcid.org/0000-0002-4278-454X




https://dx.doi.org/10.1021/acs.jproteome.0c00335
J. Proteome Res. 2020, 19, 4034−4045

**Céline Landon** − *Center for Molecular Biophysics, CBM, UPR 4301, CNRS, F-45071 Orléans Cedex 02, France;* orcid.org/0000-0002-0248-1990

Complete contact information is available at: https://pubs.acs.org/10.1021/acs.jproteome.0c00335

## Notes

The authors declare no competing financial interest.

## ■ ACKNOWLEDGMENTS

The authors acknowledge the CNRS and the "Centre Val de Loire" region for their financial support.

## ■ REFERENCES

(1) Macdonald, M. E.; Ambrose, C. M.; Duyao, M. P.; Myers, R. H.; Lin, C.; Srinidhi, L.; Barnes, G.; Taylor, S. A.; James, M.; Groot, N.; et al. A novel gene containing a trinucleotide repeat that is expanded and unstable on Huntington's disease chromosones. *Cell* **1993**, *72*, 971−983.

(2) Andrew, S. E.; Paul Goldberg, Y.; Kremer, B.; Telenius, H.; Theilmann, J.; Adam, S.; Starr, E.; Squitieri, F.; Lin, B.; Kalchman, M. A.; et al. The relationship between trinucleotide (CAG) repeat length and clinical-features of Huntingtons-Disease. *Nat. Genet.* **1993**, *4*, 398−403.

(3) Saudou, F.; Humbert, S. The Biology of Huntingtin. *Neuron* **2016**, *89*, 910−926.

(4) Carroll, J. B.; Bates, G. P.; Steffan, J.; Saft, C.; Tabrizi, S. J. Treating the whole body in Huntington's disease. *Lancet Neurol.* **2015**, *14*, 1135−1142.

(5) Bates, G. P.; Dorsey, R.; Gusella, J. F.; Hayden, M. R.; Kay, C.; Leavitt, B. R.; Nance, M.; Ross, C. A.; Scahill, R. I.; Wetzel, R.; et al. Huntington disease. *Nat. Rev. Dis. Primers* **2015**, *1*, 15005.

(6) Labbadia, J.; Morimoto, R. I. Huntington's disease: underlying molecular mechanisms and emerging concepts. *Trends Biochem. Sci.* **2013**, *38*, 378−385.

(7) McColgan, P.; Tabrizi, S. J. Huntington's disease: a clinical review. *Eur. J. Neurol.* **2018**, *25*, 24−34.

(8) Caboche, J.; Vanhoutte, P.; Boussicault, L.; Roze, E.; Betuing, S. In *Handbook of Behavioral Neuroscience*; Steiner, H., Tseng, K. Y., Eds.; Elsevier, 2016; Vol. *24*.

(9) Illarioshkin, S. N.; Klyushnikov, S. A.; Vigont, V. A.; Seliverstov, Y. A.; Kaznacheyeva, E. V. Molecular Pathogenesis in Huntington's Disease. *Biochemistry* **2018**, *83*, 1030−1039.

(10) Dumas, M.-E.; Davidovic, L. Metabolic Profiling and Phenotyping of Central Nervous System Diseases: Metabolites Bring Insights into Brain Dysfunctions. *J. Neuroimmune Pharmacol.* **2015**, *10*, 402−424.

(11) Graham, S. F.; Kumar, P. K.; Bjorndahl, T.; Han, B.; Yilmaz, A.; Sherman, E.; Bahado-Singh, R. O.; Wishart, D.; Mann, D.; Green, B. D. Metabolic signatures of Huntington's disease (HD): H-1 NMR analysis of the polar metabolome in post-mortem human brain. *Biochim. Biophys. Acta, Mol. Basis Dis.* **2016**, *1862*, 1675−1684.

(12) Patassini, S.; Begley, P.; Xu, J.; Church, S. J.; Reid, S. J.; Kim, E. H.; Curtis, M. A.; Dragunow, M.; Waldvogel, H. J.; Snell, R. G.; et al. Metabolite mapping reveals severe widespread perturbation of multiple metabolic processes in Huntington's disease human brain. *Biochim. Biophys. Acta, Mol. Basis Dis.* **2016**, *1862*, 1650−1662.

(13) Pépin, J.; Francelle, L.; Carrillo-de Sauvage, M.-A.; de Longprez, L.; Gipchtein, P.; Cambon, K.; Valette, J.; Brouillet, E.; Flament, J. In vivo imaging of brain glutamate defects in a knock-in mouse model of Huntington's disease. *Neuroimage* **2016**, *139*, 53−64.

(14) Unschuld, P. G.; Edden, R. A. E.; Carass, A.; Liu, X.; Shanahan, M.; Wang, X.; Oishi, K.; Brandt, J.; Bassett, S. S.; Redgrave, G. W.; et al. Brain metabolite alterations and cognitive dysfunction in early Huntington's disease. *Mov. Disord.* **2012**, *27*, 895−902.

(15) Mastrokolias, A.; Pool, R.; Mina, E.; Hettne, K. M.; van Duijn, E.; van der Mast, R. C.; van Ommen, G.; t Hoen, P. A. C.; Prehn, C.; Adamski, J.; et al. Integration of targeted metabolomics and transcriptomics identifies deregulation of phosphatidylcholine metabolism in Huntington's disease peripheral blood samples. *Metabolomics* **2016**, *12*, 137.

(16) Cheng, M.-L.; Chang, K.-H.; Wu, Y.-R.; Chen, C.-M. Metabolic disturbances in plasma as biomarkers for Huntington's disease. *J. Nutr. Biochem.* **2016**, *31*, 38−44.

(17) Verwaest, K. A.; Vu, T. N.; Laukens, K.; Clemens, L. E.; Nguyen, H. P.; Van Gasse, B.; Martins, J. C.; Van der Linden, A.; Dommisse, R. H-1 NMR based metabolomics of CSF and blood serum: A metabolic profile for a transgenic rat model of Huntington disease. *Biochim. Biophys. Acta, Mol. Basis Dis.* **2011**, *1812*, 1371−1379.

(18) Pont, L.; Benavente, F.; Jaumot, J.; Tauler, R.; Alberch, J.; Ginés, S.; Barbosa, J.; Sanz-Nebot, V. Metabolic profiling for the identification of Huntington biomarkers by on-line solid-phase extraction capillary electrophoresis mass spectrometry combined with advanced data analysis tools. *Electrophoresis* **2016**, *37*, 795−808.

(19) Ismailoglu, I.; Chen, Q.; Popowski, M.; Yang, L.; Gross, S. S.; Brivanlou, A. H. Huntingtin protein is essential for mitochondrial metabolism, bioenergetics and structure in murine embryonic stem cells. *Dev. Biol.* **2014**, *391*, 230−240.

(20) Zacharoff, L.; Tkac, I.; Song, Q.; Tang, C.; Bolan, P. J.; Mangia, S.; Henry, P.-G.; Li, T.; Dubinsky, J. M. Cortical metabolites as biomarkers in the R6/2 model of Huntington's disease. *J. Cereb. Blood Flow Metab.* **2012**, *32*, 502−514.

(21) Chang, K. L.; New, L. S.; Mal, M.; Goh, C. W.; Aw, C. C.; Browne, E. R.; Chan, E. C. Y. Metabolic Profiling of 3-Nitropropionic Acid Early-Stage Huntington's Disease Rat Model Using Gas Chromatography Time-of-Flight Mass Spectrometry. *J. Proteome Res.* **2011**, *10*, 2079−2087.

(22) Tsang, T. M.; Haselden, J. N.; Holmes, E. Metabonomic Characterization of the 3-Nitropropionic Acid Rat Model of Huntington's Disease. *Neurochem. Res.* **2009**, *34*, 1261−1271.

(23) Skene, D. J.; Middleton, B.; Fraser, C. K.; Pennings, J. L. A.; Kuchel, T. R.; Rudiger, S. R.; Bawden, C. S.; Morton, A. J. Metabolic profiling of presymptomatic Huntington's disease sheep reveals novel biomarkers. *Sci. Rep.* **2017**, *7*, 43030.

(24) Singh, V.; Sharma, R. K.; Athilingam, T.; Sinha, P.; Sinha, N.; Thakur, A. K. NMR Spectroscopy-based Metabolomics of Drosophila Model of Huntington's Disease Suggests Altered Cell Energetics. *J. Proteome Res.* **2017**, *16*, 3863−3872.

(25) Rosas-Arellano, A.; Estrada-Mondragón, A.; Piña, R.; Mantellero, C.; Castro, M. The Tiny Drosophila Melanogaster for the Biggest Answers in Huntington's Disease. *Int. J. Mol. Sci.* **2018**, *19*, 2398.

(26) Marsh, J. L.; Thompson, L. M. Drosophila in the study of neurodegenerative disease. *Neuron* **2006**, *52*, 169−178.

(27) McGurk, L.; Berson, A.; Bonini, N. M. Drosophila as an In Vivo Model for Human Neurodegenerative Disease. *Genetics* **2015**, *201*, 377−402.

(28) Lewis, E. A.; Smith, G. A. Using Drosophila models of Huntington's disease as a translatable tool. *J. Neurosci. Methods* **2016**, *265*, 89−98.

(29) Lin, D. M.; Goodman, C. S. Ectopic and increased expression of fasciclin-II alters motoneuron growth cone guidance. *Neuron* **1994**, *13*, 507−523.

(30) Steffan, J. S.; Bodai, L.; Pallos, J.; Poelman, M.; McCampbell, A.; Apostol, B. L.; Kazantsev, A.; Schmidt, E.; Zhu, Y.-Z.; Greenwald, M.; et al. Histone deacetylase inhibitors arrest polyglutamine-dependent neurodegeneration in Drosophila. *Nature* **2001**, *413*, 739−743.

(31) Ott, S.; Vishnivetskaya, A.; Malmendal, A.; Crowther, D. C. Metabolic changes may precede proteostatic dysfunction in a Drosophila model of amyloid beta peptide toxicity. *Neurobiol. Aging* **2016**, *41*, 39−52.

(32) Sarup, P.; Pedersen, S. M. M.; Nielsen, N. C.; Malmendal, A.; Loeschcke, V. The Metabolic Profile of Long-Lived Drosophila melanogaster. *PLoS One* **2012**, *7*, No. e47461.

(33) Zhang, Z.-M.; Chen, S.; Liang, Y.-Z. Baseline correction using adaptive iteratively reweighted penalized least squares. *Analyst* **2010**, *135*, 1138−1146.
(34) Bloemberg, T. G.; Gerretzen, J.; Wouters, H. J. P.; Gloerich, J.; van Dael, M.; Wessels, H. J. C. T.; van den Heuvel, L. P.; Eilers, P. H. C.; Buydens, L. M. C.; Wehrens, R. Improved parametric time warping for proteomics. *Chemom. Intell. Lab. Syst.* **2010**, *104*, 65−74.
(35) Wehrens, R. *Chemometrics with R: Multivariate Data Analysis in the Natural Sciences and Life Sciences*; Springer-Verlag Berlin Heidelberg GmbH & Co. K, 2011; pp 20−31.
(36) Jacob, D.; Deborde, C.; Lefebvre, M.; Maucourt, M.; Moing, A. NMRProcFlow: a graphical and interactive tool dedicated to 1D spectra processing for NMR-based metabolomics. *Metabolomics* **2017**, *13*, 36.
(37) De Meyer, T.; Sinnaeve, D.; Van Gasse, B.; Tsiporkova, E.; Rietzschel, E. R.; De Buyzere, M. L.; Gillebert, T. C.; Bekaert, S.; Martins, J. C.; Van Criekinge, W. NMR-based characterization of metabolic alterations in hypertension using an adaptive, intelligent binning algorithm. *Anal. Chem.* **2008**, *80*, 3783−3790.
(38) Giacomoni, F.; Le Corguille, G.; Monsoor, M.; Landi, M.; Pericard, P.; Petera, M.; Duperier, C.; Tremblay-Franco, M.; Martin, J.-F.; Jacob, D.; et al. Workflow4Metabolomics: a collaborative research infrastructure for computational metabolomics. *Bioinformatics* **2015**, *31*, 1493−1495.
(39) Trygg, J.; Holmes, E.; Lundstedt, T. Chemometrics in metabonomics. *J. Proteome Res.* **2007**, *6*, 469−479.
(40) Colquhoun, D. An investigation of the false discovery rate and the misinterpretation of p-values. *R. Soc. Open Sci.* **2014**, *1*, 140216.
(41) Wishart, D. S.; Feunang, Y. D.; Marcu, A.; Guo, A. C.; Liang, K.; Vazquez-Fresno, R.; Sajed, T.; Johnson, D.; Li, C.; Karu, N.; et al. HMDB 4.0: the human metabolome database for 2018. *Nucleic Acids Res.* **2018**, *46*, D608−D617.
(42) Ulrich, E. L.; Akutsu, H.; Doreleijers, J. F.; Harano, Y.; Ioannidis, Y. E.; Lin, J.; Livny, M.; Mading, S.; Maziuk, D.; Miller, Z.; et al. BioMagResBank. *Nucleic Acids Res.* **2008**, *36*, D402−D408.
(43) Xia, J.; Sinelnikov, I. V.; Han, B.; Wishart, D. S. MetaboAnalyst 3.0-making metabolomics more meaningful. *Nucleic Acids Res.* **2015**, *43*, W251−W257.
(44) Liévens, J.-C.; Rival, T.; Iché, M.; Chneiweiss, H.; Birman, S. Expanded polyglutamine peptides disrupt EGF receptor signaling and glutamate transporter expression in Drosophila. *Hum. Mol. Genet.* **2005**, *14*, 713−724.
(45) Liévens, J.-C.; Iché, M.; Laval, M.; Faivre-Sarrailh, C.; Birman, S. AKT-sensitive or insensitive pathways of toxicity in glial cells and neurons in Drosophila models of Huntington's disease. *Hum. Mol. Genet.* **2008**, *17*, 882−894.
(46) Pallos, J.; Bodai, L.; Lukacsovich, T.; Purcell, J. M.; Steffan, J. S.; Thompson, L. M.; Marsh, J. L. Inhibition of specific HDACs and sirtuins suppresses pathogenesis in a Drosophila model of Huntington's disease. *Hum. Mol. Genet.* **2008**, *17*, 3767−3775.
(47) Zhang, S.; Feany, M. B.; Saraswati, S.; Littleton, J. T.; Perrimon, N. Inactivation of Drosophila Huntingtin affects long-term adult functioning and the pathogenesis of a Huntington's disease model. *Dis. Models Mech.* **2009**, *2*, 247−266.
(48) Besson, M. T.; Alegría, K.; Garrido-Gerter, P.; Barros, L. F.; Liévens, J.-C. Enhanced Neuronal Glucose Transporter Expression Reveals Metabolic Choice in a HD Drosophila Model. *PLoS One* **2015**, *10*, No. e0118765.
(49) Besson, M.-T.; Dupont, P.; Fridell, Y.-W. C.; Liévens, J.-C. Increased energy metabolism rescues glia-induced pathology in a Drosophila model of Huntington's disease. *Hum. Mol. Genet.* **2010**, *19*, 3372−3382.
(50) Tsang, T. M.; Woodman, B.; McLoughlin, G. A.; Griffin, J. L.; Tabrizi, S. J.; Bates, G. P.; Holmes, E. Metabolic characterization of the R6/2 transgenic mouse model of Huntington's disease by high-resolution MAS (1)H NMR spectroscopy. *J. Proteome Res.* **2006**, *5*, 483−492.
(51) Graham, S. F.; Kumar, P.; Bahado-Singh, R. O.; Robinson, A.; Mann, D.; Green, B. D. Novel Metabolite Biomarkers of Huntington's Disease As Detected by High-Resolution Mass Spectrometry. *J. Proteome Res.* **2016**, *15*, 1592−1601.
(52) Behrens, P. F.; Franz, P.; Woodman, B.; Lindenberg, K. S.; Landwehrmeyer, G. B. Impaired glutamate transport and glutamate-glutamine cycling: downstream effects of the Huntington mutation. *Brain* **2002**, *125*, 1908−1922.
(53) Joyner, P. M.; Matheke, R. M.; Smith, L. M.; Cichewicz, R. H. Probing the Metabolic Aberrations Underlying Mutant Huntingtin Toxicity in Yeast and Assessing Their Degree of Preservation in Humans and Mice. *J. Proteome Res.* **2010**, *9*, 404−412.
(54) Naia, L.; Ribeiro, M.; Rodrigues, J.; Duarte, A. I.; Lopes, C.; Rosenstock, T. R.; Hayden, M. R.; Rego, A. C. Insulin and IGF-1 regularize energy metabolites in neural cells expressing full-length mutant huntingtin. *Neuropeptides* **2016**, *58*, 73−81.
(55) Papsdorf, K.; Kaiser, C. J. O.; Drazic, A.; Grotzinger, S. W.; Haessner, C.; Eisenreich, W.; Richter, K. Polyglutamine toxicity in yeast induces metabolic alterations and mitochondrial defects. *BMC Genomics* **2015**, *16*, 662.
(56) Cheng, M.-L.; Chang, K.-H.; Wu, Y.-R.; Chen, C.-M. Metabolic disturbances in plasma as biomarkers for Huntington's disease. *J. Nutr. Biochem.* **2016**, *31*, 38−44.
(57) Mochel, F.; Charles, P.; Seguin, F.; Barritault, J.; Coussieu, C.; Perin, L.; Le Bouc, Y.; Gervais, C.; Carcelain, G.; Vassault, A.; et al. Early Energy Deficit in Huntington Disease: Identification of a Plasma Biomarker Traceable during Disease Progression. *PLoS One* **2007**, *2*, No. e647.
(58) Sturrock, A.; Laule, C.; Wyper, K.; Milner, R. A.; Decolongon, J.; Santos, R. D.; Coleman, A. J.; Carter, K.; Creighton, S.; Bechtel, N.; et al. A Longitudinal Study of Magnetic Resonance Spectroscopy Huntington's Disease Biomarkers. *Mov. Disord.* **2015**, *30*, 393−401.
(59) Tkac, I.; Dubinsky, J. M.; Keene, C. D.; Gruetter, R.; Low, W. C. Neurochemical changes in Huntington R6/2 mouse striatum detected by in vivo H-1 NMR spectroscopy. *J. Neurochem.* **2007**, *100*, 1397−1406.
(60) van den Bogaard, S. J. A.; Dumas, E. M.; Teeuwisse, W. M.; Kan, H. E.; Webb, A.; Roos, R. A. C.; van der Grond, J. Exploratory 7-Tesla magnetic resonance spectroscopy in Huntington's disease provides in vivo evidence for impaired energy metabolism. *J. Neurol.* **2011**, *258*, 2230−2239.
(61) Tkac, I.; Henry, P.-G.; Zacharoff, L.; Wedel, M.; Gong, W.; Deelchand, D. K.; Li, T.; Dubinsky, J. M. Homeostatic adaptations in brain energy metabolism in mouse models of Huntington disease. *J. Cereb. Blood Flow Metab.* **2012**, *32*, 1977−1988.
(62) Mochel, F.; Haller, R. G. Energy deficit in Huntington disease: why it matters. *J. Clin. Invest.* **2011**, *121*, 493−499.
(63) Dubinsky, J. M. Towards an Understanding of Energy Impairment in Huntington's Disease Brain. *J. Huntington's Dis.* **2017**, *6*, 267−302.
(64) Polyzos, A. A.; Lee, D. Y.; Datta, R.; Hauser, M.; Budworth, H.; Holt, A.; Mihalik, S.; Goldschmidt, P.; Frankel, K.; Trego, K.; et al. Metabolic Reprogramming in Astrocytes Distinguishes Region-Specific Neuronal Susceptibility in Huntington Mice. *Cell Metab.* **2019**, *29*, 1258−1273.
(65) Toczek, M.; Zielonka, D.; Zukowska, P.; Marcinkowski, J. T.; Slominska, E.; Isalan, M.; Smolenski, R. T.; Mielcarek, M. An impaired metabolism of nucleotides underpins a novel mechanism of cardiac remodeling leading to Huntington's disease related cardiomyopathy. *Biochim. Biophys. Acta, Mol. Basis Dis.* **2016**, *1862*, 2147−2157.
(66) Gruber, B.; Kłaczkow, G.G.; Jaworska, M.; Krzysztoń-Russjan, J.; Anuszewska, E. L.; Zielonka, D.; Klimberg, A.; Marcinkowski, J. T. Huntington' disease—imbalance of amino acid levels in plasma of patients and mutation carriers. *Ann. Agric. Environ. Med.* **2013**, *20*, 779−783.
(67) Zacharoff, L.; Tkac, I.; Song, Q.; Tang, C.; Bolan, P. J.; Mangia, S.; Henry, P.-G.; Li, T.; Dubinsky, J. M. Cortical metabolites as biomarkers in the R6/2 model of Huntington's disease. *J. Cereb. Blood Flow Metab.* **2012**, *32*, 502−514.


https://dx.doi.org/10.1021/acs.jproteome.0c00335
J. Proteome Res. 2020, 19, 4034−4045

(68) Peng, Q.; Wu, B.; Jiang, M.; Jin, J.; Hou, Z.; Zheng, J.; Zhang, J.; Duan, W. Characterization of Behavioral, Neuropathological, Brain Metabolic and Key Molecular Changes in zQ175 Knock-In Mouse Model of Huntington's Disease. *PLoS One* **2016**, *11*, No. e0148839.
(69) Menzie, J.; Pan, C.; Prentice, H.; Wu, J.-Y. Taurine and central nervous system disorders. *Amino Acids* **2014**, *46*, 31−46.
(70) Jakaria, M.; Azam, S.; Haque, M. E.; Jo, S.-H.; Uddin, M. S.; Kim, I.-S.; Choi, D.-K. Taurine and its analogs in neurological disorders: Focus on therapeutic potential and molecular mechanisms. *Redox Biol.* **2019**, *24*, 101223.
(71) Tadros, M. G.; Khalifa, A. E.; Abdel-Naim, A. B.; Arafa, H. M. M. Neuroprotective effect of taurine in 3-nitropropionic acid-induced experimental animal model of Huntington's disease phenotype. *Pharmacol., Biochem. Behav.* **2005**, *82*, 574−582.
(72) Zabel, C.; Mao, L.; Woodman, B.; Rohe, M.; Wacker, M. A.; Kläre, Y.; Koppelstätter, A.; Nebrich, G.; Klein, O.; Grams, S.; et al. A Large Number of Protein Expression Changes Occur Early in Life and Precede Phenotype Onset in a Mouse Model for Huntington Disease. *Mol. Cell. Proteomics* **2009**, *8*, 720−734.
(73) Perluigi, M.; Poon, H. F.; Maragos, W.; Pierce, W. M.; Klein, J. B.; Calabrese, V.; Cini, C.; De Marco, C.; Butterfield, D. A. Proteomic analysis of protein expression and oxidative modification in R6/2 transgenic mice. *Mol. Cell. Proteomics* **2005**, *4*, 1849−1861.
(74) Naia, L.; Cunha-Oliveira, T.; Rodrigues, J.; Rosenstock, T. R.; Oliveira, A.; Ribeiro, M.; Carmo, C.; Oliveira-Sousa, S. I.; Duarte, A. I.; Hayden, M. R.; et al. Histone Deacetylase Inhibitors Protect Against Pyruvate Dehydrogenase Dysfunction in Huntington's Disease. *J. Neurosci.* **2017**, *37*, 2776−2794.


https://dx.doi.org/10.1021/acs.jproteome.0c00335
*J. Proteome Res.* 2020, 19, 4034−4045